

Eco-Friendly Adsorptive Removal of Chromium From Water and Wastewater by Nano Sodium Bentonite

Maryam Omidvar-Motlagh, Zarrin Es'haghi, Hasan Ali Hosseini*

Department of Chemistry, Payame Noor University, 19395-4697, Tehran, Iran

Received: 3 September 2023 Accepted: 8 October 2023

DOI: [10.30473/ijac.2023.69100.1274](https://doi.org/10.30473/ijac.2023.69100.1274)

Abstract

Contamination of water sources with chromium has become a pervasive global problem due to its wide use in industry. In this research, low-cost commercial sodium bentonite and synthesized nano bentonite were used to remove chromium ions from aqueous solutions along with electro thermal atomic absorption spectroscopy (ETAAS) and Ultraviolet-Visible Spectrophotometry (UV-Vis) were used. The morphology of the bentonite samples was studied using XRD, FTIR and scanning electron microscope (SEM) analyzes. To screen the relative importance of variables, parameters including pH, adsorption time, amount of adsorbent, volume of desorption solvent and stirring speed were studied using the Plackett Burman Design (PBD) using the Minitab 20 software. In the following, optimization was performed by using the central composite design (CCD), and the responses were evaluated. The calibration curve was plotted by drawing the absorbance against standard concentration. The linear dynamic range of $0.003\text{-}100\ \mu\text{g L}^{-1}$ (DLR) and the correlation coefficient (R^2) of 0.999 were obtained for chromium. Limit of detection (LOD) and limit of quantification (LOQ) for chromium were obtained equal to 0.002 and $0.0039\ \mu\text{g L}^{-1}$, respectively. The relative standard deviation (RSD) of 6.93% and the relative recovery for chromium in real samples were obtained in the range 96.041% to 103.445% for ETAAS method. The values of detection limit (LOD) and limit of quantification (LOQ) by UV-Vis method were 0.007 and $0.021\ \mu\text{g L}^{-1}$ respectively, and the dynamic linear range was (DLR) $0.05\text{-}50.00\ \mu\text{g L}^{-1}$ with a correlation coefficient (R^2) 0.998. The relative standard deviation (RSD) was 14.27% and the relative recovery of this method in real samples was attained from 95.103% to 103.692%.

Keywords

Electrothermal atomic absorption spectroscopy; Ultraviolet-Visible Spectrophotometry; Nano sodium bentonite; Chromium.

1. INTRODUCTION

In order to protect public health, it is necessary to control and monitor the concentration of pollutants in water resources [1]. Chromium is a metallic element that is found naturally in rocks, soils, plants, animals, gases and volcanic dust [2]. In addition to natural resources, it is one of the major industrial wastes. In general, chromium exists in two forms; trivalent (Cr (III)) and hexavalent chromium (Cr (VI)) [1, 2]. According to national standards of Iran (No. 1053), maximum contaminant level of total chromium in drinking water is $50\ \mu\text{g L}^{-1}$ (50 ppb) for public waters [3]. Biological treatment is one of the available techniques for chromium removal [4], chemical methods, reduction [5, 6] and adsorption

approaches [7] can also be effective methods for chromium elimination. Most of these methods are expensive and time consuming. In the recent years, the removal of various groundwater pollutants has been carried out using nano-adsorbents. Higher reactive surface, faster and more complete reactions are among the advantages of nano-adsorbents including iron magnetic adsorbents [8]. However, there are issues such as low stability, limitations imposed by high reactivity and aggregation of magnetic particles [9]. Lately, to increase the dispersion of Fe_3O_4 nanoparticles, porous materials have been used as mechanical supports [10].

Bentonite is a low-cost traditional adsorbent that is used for the removal of heavy metals from

* Corresponding author:

H. Ali Hosseini; E-mail: shahosseini57@pnu.ac.ir

wastewater due to its abundance, high absorbance, unique structural properties, chemical and mechanical stability, and high potential [11]. Bentonite has been used to remove metal ions based on adsorption and ion exchange mechanisms due to its specific surface area and relatively high cation exchange capacity [11].

Bentonite with chemical Formula of $(\text{Na, Ca}) (\text{Al, Mg}) (\text{Si}_4\text{O}_{10})_3 (\text{OH})_6 n\text{H}_2\text{O}$ is a mineral substance from the category of clays or pseudo-clays. It generally contains montmorillonite and a small amount of beidellite. Therefore, the clay that has 85-90% of montmorillonite mineral is bentonite, and the properties and quality of bentonite vary according to the amount of montmorillonite. The structure of bentonite is aluminosilicate which is a three-layer silicate and has two tetrahedral layers and one octahedral layer (Fig. 1). In the tetrahedral form, the silica unit is the tetrahedral unit and the common unit of all clay minerals, and it is a pyramidal tetrahedron in which one silicon atom is surrounded by four oxygen atoms. The tetrahedral units are connected to each other in a planar way and form a hexagonal structure that holes are formed in between this hexagonal structure. And if sufficient electric charge is provided on the surface of oxygen, they provide a suitable place to stabilize interlayer ions for the clay surface.

In the octahedron form, the cations in bentonite are surrounded by six hydroxyl units in a planar form in an octahedron. Between the octahedral and tetrahedral planes, the connection takes place through the sharing of the oxygen at the vertex of the tetrahedral unit and the placement of the central element in the aluminum octahedral unit. The existence of weak van der Waals bonds between bentonite layers causes them to easily slide on each other. Therefore, bentonite feels greasy. Also, the absorption of water by bentonite particles in the aqueous environment is between seven to twenty times their volume and they swell. The main reason for swelling is the absorption of water in the surface layers due to the hydration of exchangeable cations and the separation of the network layers in the interior as a result of the similar repulsion force, which is called osmotic swelling [12- 14].

According to their characteristics, bentonites are mainly divided into two categories, sodium-containing or swollen bentonites and the second type, calcium-containing or non-swollen bentonites. Sodium bentonites have the ability to

absorb water up to several times their normal volume, and due to the excellent colloidal properties of this compound, it is often used in geotechnical and environmental research and drilling fluid for oil and gas wells [15-18].

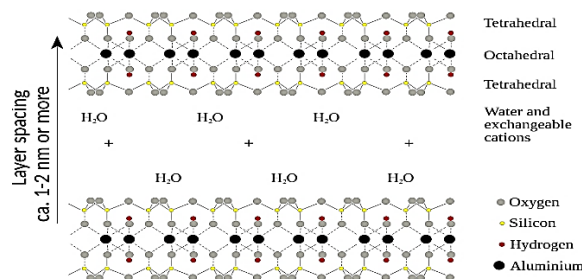


Fig. 1. Bentonite structure (Wikipedia)

Calcium-containing bentonites adsorb ions in solution and can adsorb fats and oils in an environment. This material is the main composition of the earth's crust and is considered one of the first industrial cleaning materials. Bentonites can be activated. Active bentonite refers to soils that are modified with a chemical substance. The activation of bentonites is mostly by using salt water solution to exchange calcium ions with sodium, which increases the swelling and suspend ability properties of bentonites. It is also possible to convert the calcium bentonite to the sodium type. For this purpose, calcium cations are interlayered. Of course, this substitution depends on the temperature, time and amount of sodium salt and is never complete [15-18].

This paper aims to evaluate the effect of sodium bentonite on chromium ions adsorption. The experimental results and adsorption process are explained by the variation of effective factors. The effect of cation replacement on the absorption of heavy metals is rarely investigated in detail, it is investigated in this research. This study on the adsorption mechanism of chromium ions by sodium bentonite has certain significance for modified clay minerals applications.

2. EXPERIMENTAL

2.1. Chemicals

Sodium bentonite, commercial types; Z.B (type 1), and APIF (type 2), obtained from Ferdous and Qain clay mines, South Khorasan province, Iran. Sodium chloride (purity; 99%), sulfuric acid (purity;97%), nitric acid (purity;65%), acetic acid glacial, ethanol (purity $\geq 99.9\%$), chromium standard solution (purity;1000 mgL^{-1}), and arsenic, nickel, lead, cobalt, cadmium, and iron

Standard Solutions (As 100 mgL^{-1}) all purchased from Merck, Germany too. The deionized water ($< 18,2 \text{ M}\Omega$) used in the experiments was Milli-Q gradient (Millipore).

2.2. Equipment

Atomic absorption spectrometer (PG Instruments Ltd, made in England) equipped with graphite furnace model PG 990 with chromium hollow cathode lamp (wavelength 357.9 nm) (Cr HCL), slit width 0.7 nm , lamp current 8 mA , background correction method BGC-D2, peak height signal processing, input speed $130 \mu\text{L}/\text{sec}$, output speed $150 \mu\text{L}/\text{sec}$, injection volume $20 \mu\text{L}$, injection speed $25 \mu\text{L}/\text{sec}$, cooling temperature 15°C were used for the analyses. Exciton model furnace with a voltage of 220 volts and a maximum temperature of 1200 degrees , an analytical balance with ALC-110.4 model ACCU LAB Sartorius group, Germany, an Explorer model XRD device from GNR, Italy with a Dectris $V=40\text{KV}$ detector, current 20 mA , a VELP Scientifica magnetic stirrer Europe model (F20520162), scanning electron microscope (SEM) device with the ability to produce images with a magnification of 10 to $300,000$ times to identify the morphology of polymer particles model Hip ace 10 PFEIFFER-Vacuum, FT-IR device (Fourier transform infrared spectroscopy) Shimadzu 8400 made in Japan, German pH meter WTW inolab level 2, spectrophotometer UV1800 Shimadzu Japan were other tools used in this research.

2.3. Preparation of acid-activated bentonite

Bentonite can be activated by using strong acids such as hydrochloric acid for enhanced surface properties and replacing the exchangeable ions of bentonite throughout chemical procedure. During acid leaching of bentonite, at first interlayer cations are substituted with H^+ ions of the acid and subsequently dissolution of structural cations occurs. This process leads to the layering of the clay structure, thereby increasing the specific surface area of the clay and its adsorption capacity.

At first, among the bentonite samples, undesirable and heterogeneous materials include quartz, zeolites, carbonates, etc. that could be visually recognized were removed.

Sodium bentonites are very sensitive to the salty environment, so a significant reduction in swelling was observed when sodium chloride solutions were replaced. The effects of salt concentration will produce higher quality bentonite, which will have a higher swelling capacity, a more obvious cation exchange capacity, exchangeable sodium percentage and specific surface area. That's why, 5 ml of 1.0 M NaCl solution was added to 1.0 g bentonite and the mixture was stirred for three hours, after that the drying process was performed in an oven at a temperature of 60°C . Subsequently, 2 mL sulfuric acid 2 M was added and stirred at 95°C for 2 hours. Next, the product was washed several times with double distilled water and it was dried at a temperature of 60°C . Particles with a diameter of about 0.8 to 1.2 mm were gained and then the obtained material were calcinated at the temperature of 200°C for one hours in the air atmosphere [19].

2.3.1. Preparation of nano bentonite

To prepare nano bentonite, sodium bentonite commercial types Z.B (type 1), and APIF (type 2), were activated according to above section. So that, about 1.6 g of activated sodium bentonite was added to 100 ml of ethanol and then it was placed under ultrasonic with a power of 50 watts for 4 hours at a temperature of 20°C . Next, the synthesized nano bentonite was dried in an oven (90°C for 24 h). Then it was calcined at 800°C for 4 hours [20].

2.3.2. Chromium measurement

0.5 g of each activated sodium bentonite samples (type 1, and type 2), and 0.5 g of nano bentonites prepared from those two sources were weighed separately and 100 ml chromium standard solution ($500 \mu\text{gL}^{-1}$) was added to each and the mixtures were shaken for 5 minutes. After completing the chromium adsorption process by the clay adsorbent, the mixture was centrifuged and the supernatant was discarded. Then, 1 mL nitric acid (0.14M) was added to each of the adsorbents in order to desorb the analyte. The steps of stirring and centrifugation were performed. In final step, the chromium concentration of the supernatant was measured using the mentioned spectroscopic methods [21].

Table 1. Factors, Symptoms and Levels for Plackett–Burman design for two types of nano-bentonites

Agents	Sign	Levels		
		-1	0	1
pH	pH	2	5.5	9
Amount of sorbent (mg)	Sorbent (mg)	2	3.5	5
Adsorption time (min)	Time(min)	10	30	50
Adsorption solvent volume (mL)	V.ads.	1	5.5	10
Stirring speed (rpm)	Rate(rpm)	100	1050	2000

Table 2. Plakett Burman Design-Minitab 20 -nano bentonite (Type 1)

StdOrder	RunOrder	PtType	Blocks	pH	Sorbent(mg)	Time(min)	V.ads. (ml)	Rate(rpm)	Result 1 (absorbance)
11	1	1	1	9	5	10	1	2000	0.757
13	2	0	1	5.5	3.5	30	5.5	1050	0.795
5	3	2	1	9	5	30	10	100	0.733
3	4	2	1	9	3.5	50	1	100	0.719
6	5	2	1	2	2	30	1	2000	0.989
12	6	1	1	2	2	50	10	100	0.928
9	7	2	1	9	2	10	10	1050	0.749
7	8	2	1	9	2	50	5.5	2000	0.787
2	9	2	1	5.5	2	10	1	100	0.932
1	10	2	1	5.5	5	50	10	2000	1.492
10	11	2	1	2	5	50	1	1050	1.994
4	12	2	1	2	3.5	10	10	2000	1.987
8	13	2	1	2	5	10	5.5	100	2.298

Table 3. Plakett Burman Design-nano bentonite (Type 2)

StdOrder	RunOrder	PtType	Blocks	pH	sorbent(mg)	time(min)	V.ads.(ml)	Rate(rpm)	Result sample2 (absorbance)
11	1	1	1	9	5	10	1	2000	0.717
13	2	0	1	5.5	3.5	30	5.5	1050	0.832
5	3	2	1	9	5	30	10	100	0.751
3	4	2	1	9	3.5	50	1	100	0.698
6	5	2	1	2	2	30	1	2000	0.996
12	6	1	1	2	2	50	10	100	0.925
9	7	2	1	9	2	10	10	1050	0.754
7	8	2	1	9	2	50	5.5	2000	0.801
2	9	2	1	5.5	2	10	1	100	0.944
1	10	2	1	5.5	5	50	10	2000	1.695
10	11	2	1	2	5	50	1	1050	1.999
4	12	2	1	2	3.5	10	10	2000	1.981
8	13	2	1	2	5	10	5.5	100	2.324

2.4. Extraction and optimization conditions

Considering that the optimization methods of one-variable-at-a-time, require spending a long time and cost, and also there is no proper understanding of the mutual effects of the variables, the optimization was done using the factorial design and the response surface methodology [22, 23].

According to previous experiences, the type of desorption solvent and desorption conditions were optimized as one factor at a time. Different solvents such as nitric acid, acetic acid, mixture of nitric and acetic acid was used, and based on the results, nitric acid was selected as the optimal

desorption solvent. In the screening design, primary tests and variables were selected, designed, tested and the optimal conditions were determined. In the following, Plackett–Burman design (PBD) used to effectively screen the most important factors. Various influential factors and designed experiments showed reliable results.

In the initial experiments of this method, the effect of factors such as: pH, amount of adsorbent, adsorption time, volume of desorption solvent and stirring speed was investigated on the extraction efficiency process. Three levels were considered for all factors (Table 1).

Plackett–Burman matrix was designed using 13 tests in Mini Tab 20 software for both samples 1 and 2 of sodium nano bentonite (Table 2 and Table 3). Each experiment was repeated 3 times.

3. STATISTICAL ANALYSIS F

The impact value of significant tested factors was performed for both samples 1 and 2 of sodium bentonite using Mini Tab 20 software (Fig 2 and 3).

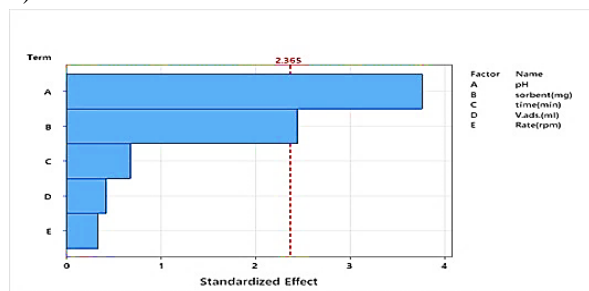


Fig. 2. Pareto chart drawn using Burman's sample 1 design in screening influencing factors

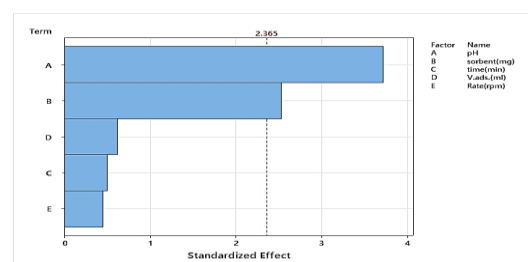


Fig. 3. Pareto chart drawn using Burman's sample 2 design in screening influencing factors

The degree of influence of each parameter on the desired response is shown along the columns. The parameters whose height is lower than the critical line drawn in the Pareto diagrams do not have a significant effect on the response and are at a significant level of 5%. And therefore, there is no need for their subsequent optimization. In addition, as it is known, the improvement of responses at high levels compared to low levels, i.e., factors including pH=2 and the amount of adsorbent at the level of 5 mg for both samples, have the greatest effect on the extraction rate of chromium, respectively. On the other hand, factors such as desorption time, volume of desorption solvent, and stirring speed, which are less than the critical line drawn, have less effect. And there is no need for re-optimization and they are considered constant in the continuation of the work [24].

The investigation of the factors influencing the response was carried out again at a significant level of 5%. The optimal value of these factors (pH) and the amount of adsorbent to perform the experiment was evaluated and optimized in the next step using the central composite design. And the effect of these factors was determined in the Mini Tab 20 software by drawing the ANOVA diagram (Fig 4 and 5).

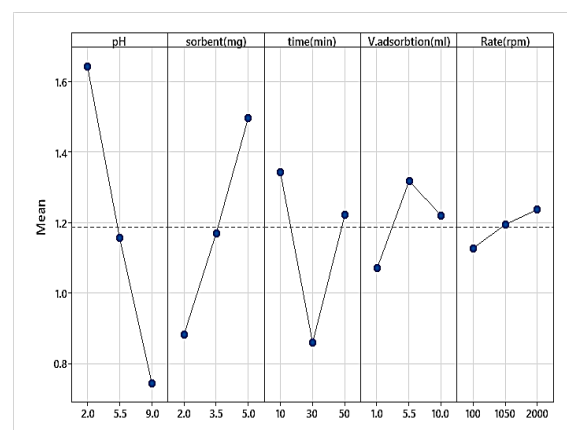


Fig. 4. The effect of the main factors on the response PBD sample1

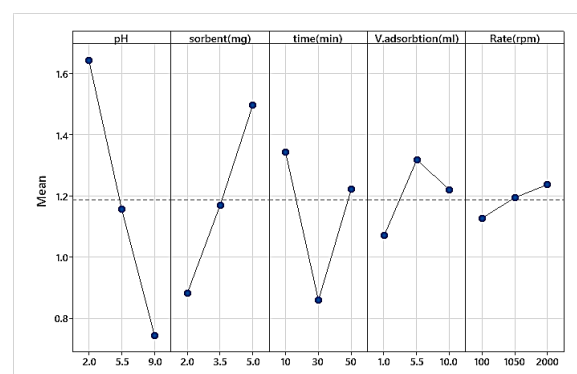


Fig. 5. The effect of the main factors on the response PBD sample2

Quadratic models (response-procedure schemes) were used to determine the optimal conditions that consider three levels for each factor in Minitab 20 software. [25, 26]

In order to obtain the best conditions, the central orthogonal composite design was used. In this plan, each factor is evaluated independently from other factors. A star design ($N_a=2^r$), a two-level factorial design and a set of repeated points are proposed in this model.

Three levels were considered for each factor using the Plackett–Burman design. The levels and effective factors of this stage are listed in Table 4.

Table 4. Factors, signs and levels of CCD

Agents	Sign	Levels		
		-1	0	1
pH	pH	1.5	3.5	5.5
Amount of sorbent (mg)	Sorbent (mg)	3.5	1.5	6.5

By using the equation $N=N_a+N_F+N_0$, the number of all tests for the implementation of Plackett–Burman design is obtained. (The number of tests in the center of the N_0 design, the number of tests related to the factorial design N_F , the star design N_a). The number of tests in the center of this project is equal to 13 for both bentonite samples 1 and 2. Tables 5a and 6a show the experiments

designed at this stage for two samples, along with 3 repetitions for each experiment and their responses. According to the results of the tables, the best response was chosen as the optimal ideal conditions to continue the work. The analysis of the results to continue the work for both samples was performed according to the optimal ideal conditions obtained from the samples in the Mini Tab 20 software. The confirmed values are at the bottom of tables 5b and 6b. According to the available results for two samples, it can be seen that there is not much difference between the two samples. Therefore, one of the samples was used to continue the process and analysis.

Table 5a. The matrix of the central composite design (CCD) for nano bentonite (Type 1)-minitab 20

StdOrder	RunOrder	PtType	Blocks	pH	sorbent(mg)	Result 1 (Abs)	% Remove
1	1	1	1	1.5	3.5	1.978	83.25%
6	2	-1	1	6.32	5	1.894	79.71%
4	3	1	1	5.5	6.5	2.061	86.74%
9	4	0	1	3.5	5	2.322	97.73%
5	5	-1	1	0.67	5	1.801	75.80%
2	6	1	1	5.5	3.5	1.737	77.65%
7	7	-1	1	3.5	2.87	1.845	77.65%
3	8	1	1	1.5	6.5	1.773	74.62%
8	9	-1	1	3.5	7.12	1.952	82.15%
12	10	0	1	3.5	5	2.321	97.69%
10	11	0	1	3.5	5	2.321	97.69%
13	12	0	1	3.5	5	2.376	100.00%
11	13	0	1	3.5	5	2.343	98.61%

Table 5b. Analysis of Variance

Source	DF	Adj SS	Adj MS	F-Value	P-Value
Model	5	0.726816	0.145363	273.32	0
Linear	2	0.013118	0.006559	12.33	0.005
2-Way Interaction	1	0.06996	0.06996	131.54	0
Error	7	0.003723	0.000532		
Lack-of-Fit	3	0.00143	0.000477	0.83	0.542
Pure Error	4	0.002293	0.000573		
Total	12	0.730539			

Model Summary

S	R-sq	R-sq(adj)	R-sq(pred)
0.0230617	99.49%	99.13%	98.12%

Table 6a. The matrix of the central composite design (CCD) -nano bentonite (Type 2)-minitab 20

StdOrder	RunOrder	PtType	Blocks	pH	sorbent(mg)	Result sample2 (Abs)	% Remove
7	1	-1	1	3.5	2.87	1.859	77.85%
3	2	1	1	1.5	6.5	1.789	74.92%
10	3	0	1	3.5	5	2.342	98.07%
4	4	1	1	5.5	6.5	2.155	90.24%
8	5	-1	1	3.5	7.12	1.973	82.62%
11	6	0	1	3.5	5	2.326	97.40%
5	7	-1	1	0.67	5	1.8999	79.56%
1	8	1	1	1.5	3.5	1.981	82.96%
13	9	0	1	3.5	5	2.333	97.70%
12	10	0	1	3.5	5	2.388	100.00%
9	11	0	1	3.5	5	2.362	98.91%
6	12	-1	1	6.32	5	1.947	81.53%
2	13	1	1	5.5	3.5	1.761	73.74%

Table 6b. Analysis of Variance

Source	DF	Adj SS	Adj MS	F-Value	P-Value
Model	5	0.675878	0.13518	268.9	0
Linear	2	0.022141	0.01107	22.02	0.001
2-Way Interaction	1	0.085849	0.08585	170.78	0
Error	7	0.003519	0.0005		
Lack-of-Fit	3	0.001002	0.00033	0.53	0.685
Pure Error	4	0.002517	0.00063		
Total	12	0.679397			
Model Summary					
S	R-sq	R-sq(adj)	R-sq(pred)		
0.0224208	99.48%	99.11%	98.37%		

4. RESULTS AND DISCUSSION

4.1. Characterization of the adsorbents

Scanning Electron Microscopic (SEM), Energy dispersive X-ray spectroscopy (EDS), X-Ray Diffraction (XRD), FT-IR spectra were taken for the prepared samples in order to investigate the characterization of the adsorbents.

4.1.1. SEM analysis for the nano-bentonite structure

The characterization of the adsorbents was done with Scanning electron microscopes. Below are the SEM and EDX images of the synthesized nano bentonite before and after trapping the chromium (Fig. 6, 7). SEM images of nano bentonite show particles with dimensions of about 12-29 nm.

4.1.2. X-ray diffraction (XRD) spectroscopy of nano bentonite before and after chromium adsorption

Materials are divided into amorphous and crystalline groups. If a peak is observed, in the XRD diagram indicates a crystalline substance. Using Scherrer equation, the size of nanocrystals (La) was calculated through X-ray diffraction spectroscopy (XRD) and with a specific wavelength (λ nanometer).

The total width of the peak at half the height of the maximum peak located at 2θ was known and measured in units of radians.

$$D = \frac{K\lambda}{\beta \cos \theta}$$

Average crystal size D (angstroms or nanometers), peak width at half maximum height β (radians) and, peak location on the horizontal axis of the diffraction pattern θ , parameter λ , wavelength $1K\alpha$ of the X-ray anode (154 nm), K value related to the crystal form factor (0.9).

To calculate the value of θ , if the horizontal axis is 2θ , it is divided by 2. The terms K and $\cos \theta$ are dimensionless in Scherrer equation. As a result, to calculate β to convert degrees to radians, the number of the peak width at half the maximum height is calculated from the following equation.

$$\beta = \frac{\pi \times FWHMD}{180}$$

Fig. 8a, 8b show the images of nano-bentonite before and after adsorbing chromium. The value of 186.86 for nano bentonite before the addition of chromium and the value of 93.02 for nano bentonite after the trapping chromium were also obtained by Scherrer equation.

Calculations and images taken by X-ray spectroscopy as well as the values calculated through Scherrer equation show that the results are in good agreement with JCPDS data for nano-bentonite before and after addition of chromium. The plans are indicated on the side of the XRD diagram.

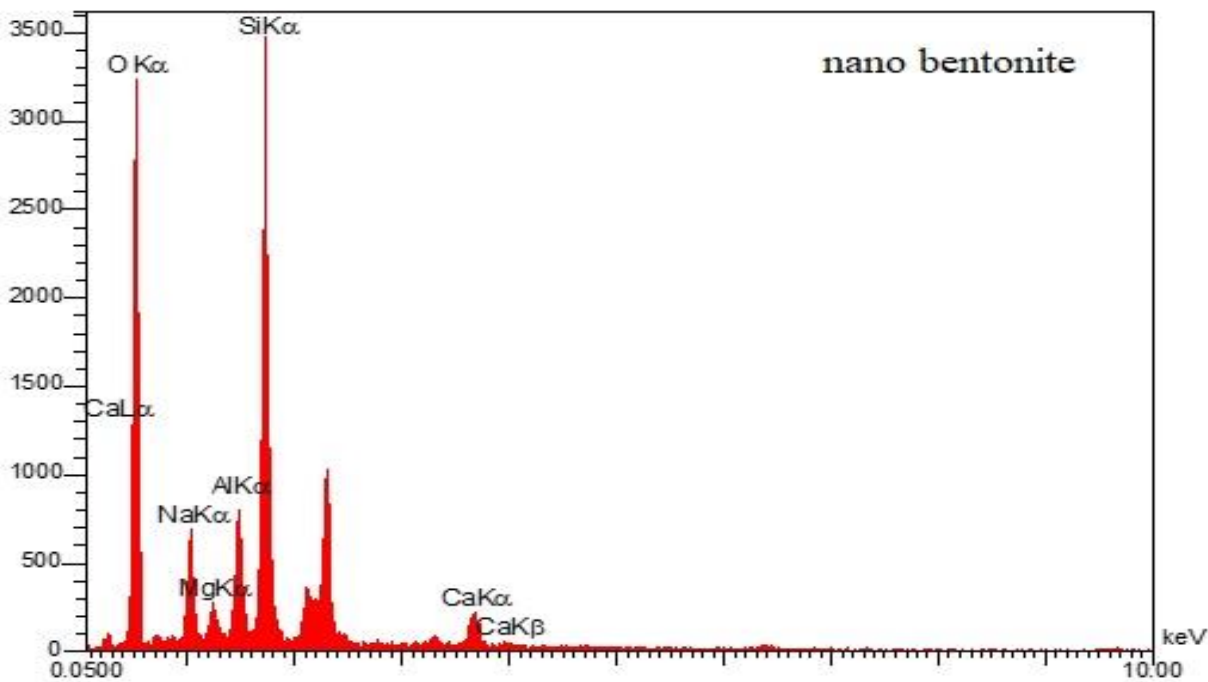
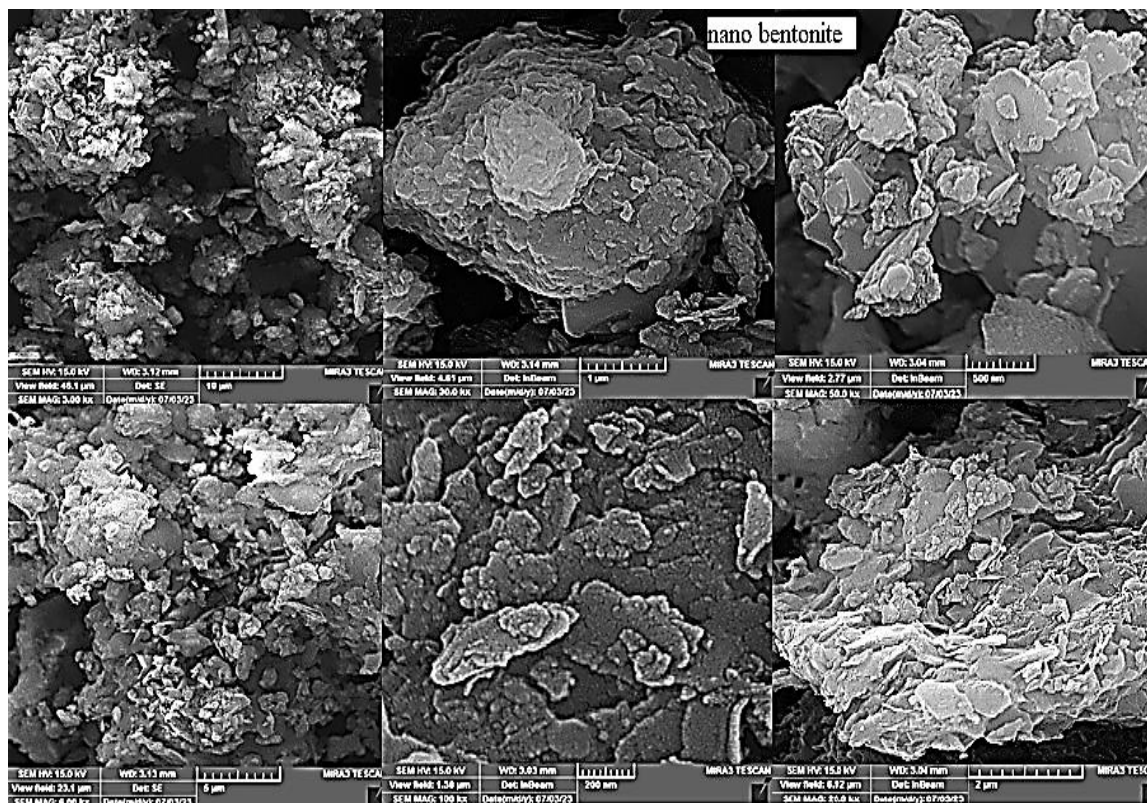


Fig. 6. SEM(up) and EDX (down) pattern image of nano Bentonite

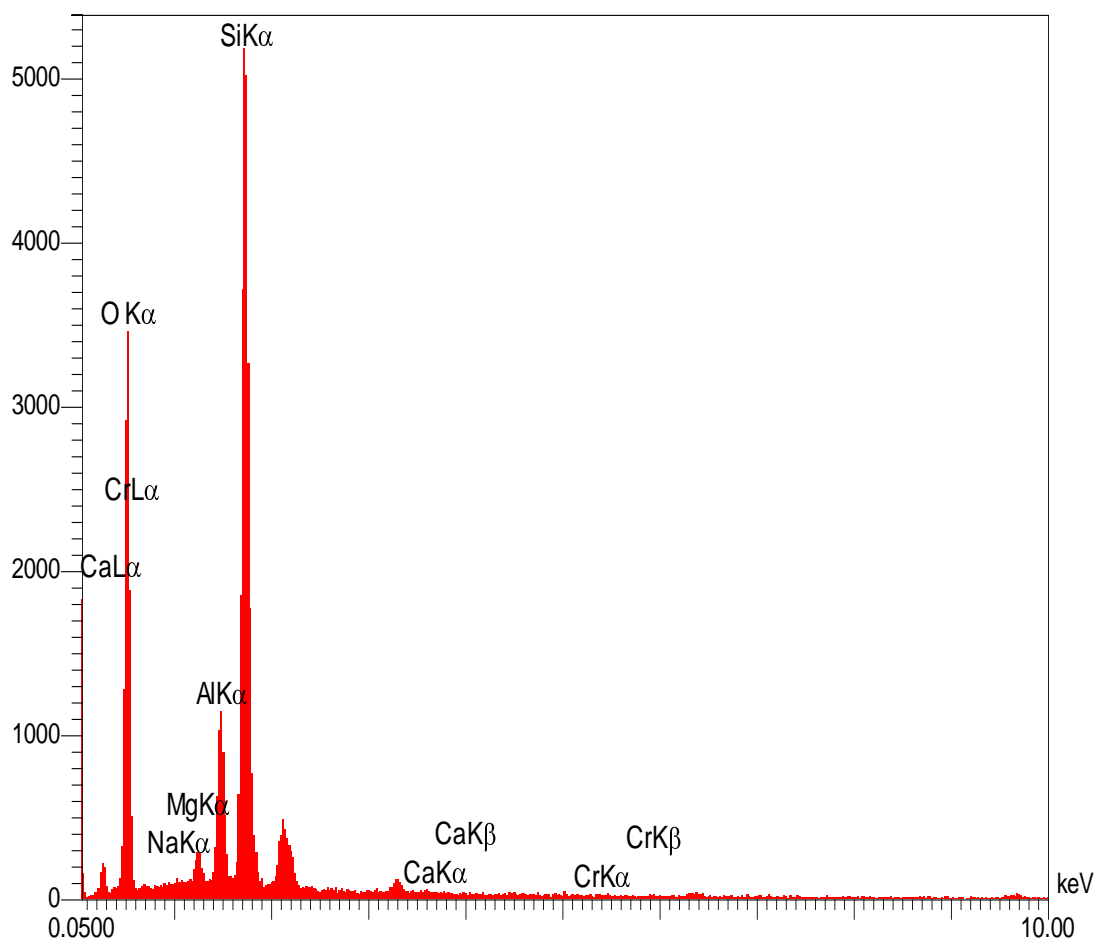
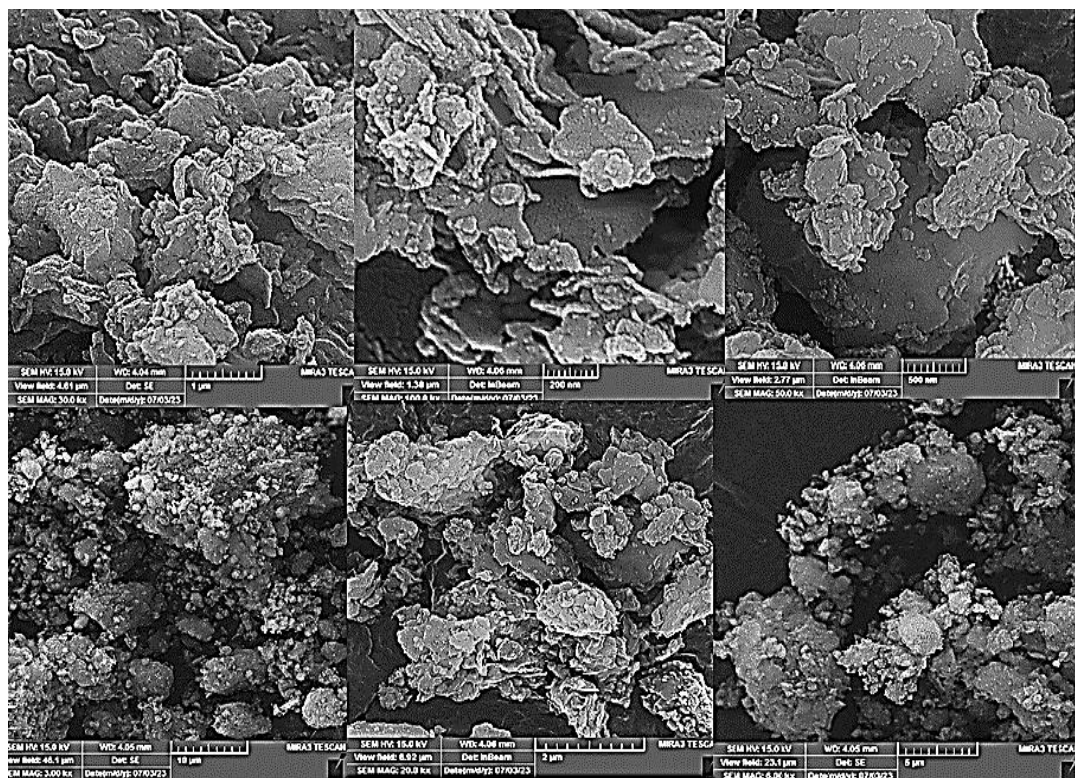


Fig. 7. SEM(uo) and EDX (down) pattern image of nano Bentonite after the chromium adsorption process

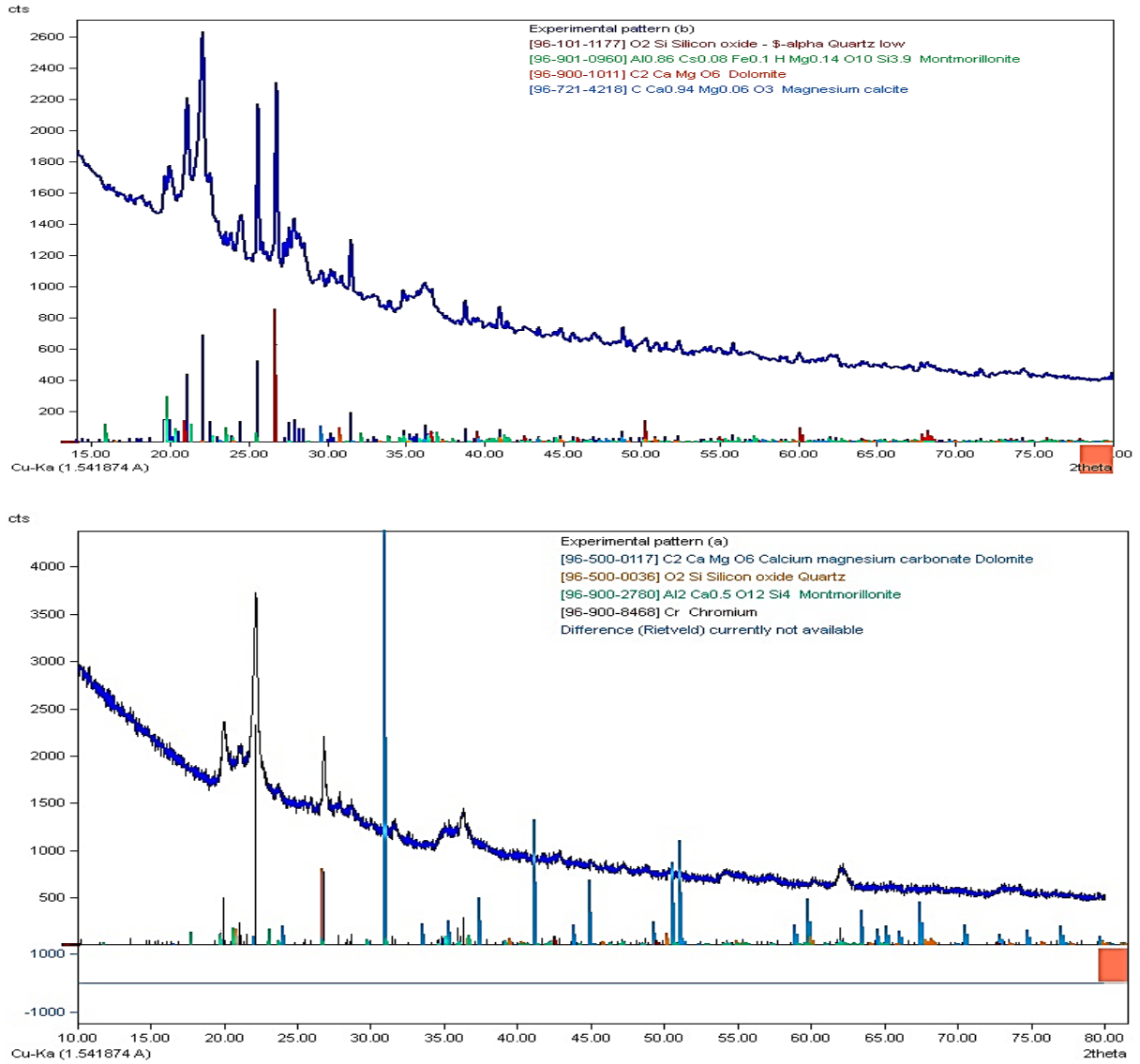


Fig. 8.(a) XRD image of nano bentonite and (b) XRD image of nano bentonite after the chromium sorption

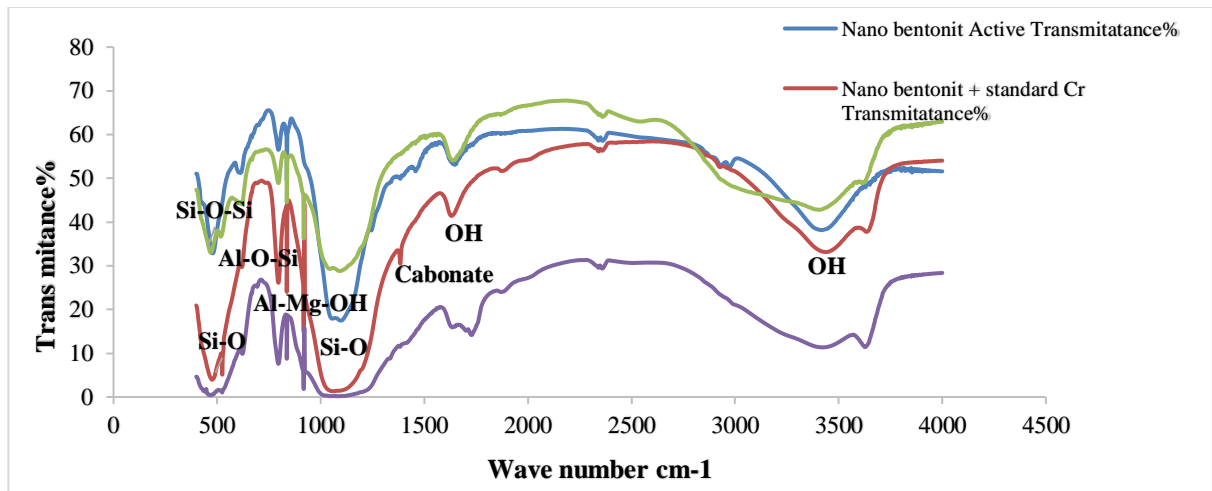


Fig. 9. FT-IR spectrum of bentonite, nano bentonite, bentonite containing adsorbed chromium and nano bentonite containing adsorbed chromium.

4.1.3. FT-IR analysis

The spectrum of the samples by Fourier-transform spectroscopy obtained based on the measurement of the coherence radiation source using time-domain measurements of the radiation. Samples were prepared by mixing and grinding an appropriate amount of each analyte powder with potassium bromide.

Bentonite is an important impure clay contains montmorillonite. The absorption bands obtained at $3436\text{-}3632\text{ cm}^{-1}$ and $1629.74\text{-}1728\text{ cm}^{-1}$ are related to the stretching and bending vibrations of the OH group of the water molecules that are adsorbed on the bentonite surface. The peak around 463 cm^{-1} corresponds to the Si-O-Si bending vibration, which is related to the Si-O tetrahedral state [27, 28]. The peak at 1475 cm^{-1} shows the presence of carbonate [29]. Vibrations observed in $1029\text{-}1044\text{ cm}^{-1}$ corresponds to the Si-O group, the peak at 524 cm^{-1} is due to bending vibration and the peak at 796 cm^{-1} corresponds to the stretching vibration is Al-O-Si [30, 31]. Finally, the peak observed at 836 cm^{-1} belongs to the Al-Mg-OH group [32] (Fig. 9).

4.2. Method validation

Calibration curve of chromium measured by ETAAS within the concentration range from 0.003 to $100\text{ }\mu\text{gL}^{-1}$ is shown in Fig. 10. The optimal conditions in which the calibration curve

is drawn are 5 mg of adsorbent, extraction time of 10 minutes , $\text{pH} = 3.5$, volume of desorption solvent of 5.5 ml , and stirring speed of 100 rpm .

The linearity of the curve was obtained in the range of 0.003 to $100\text{ }\mu\text{gL}^{-1}$. The linear equation of calibration was ($Y = 0.0253 X + 0.0578$, $R^2 = 0.999$).

The method detection limit value was found $0.0020\text{ }\mu\text{gL}^{-1}$ (± 0.0001). The limit of quantification was found to be $0.0039\text{ }\mu\text{gL}^{-1}$ (± 0.0001). The standard deviation was 7.5×10^{-5} , and the RSD value was 6.93% . Using the flexible Error bar tool, the standard error value of data measurement was determined on the calibration chart.

Calibration curve of chromium measured by UV-Vis within the concentration range from 0.05 to $50\text{ }\mu\text{gL}^{-1}$ is shown in Fig. 11. The linear calibration equation for UV-Vis method $y = 0.0273x + 0.0097$, $R^2 = 0.998$, $\text{LOD} = 0.007$, $\text{LOQ} = 0.021$, standard deviation $= 0.0007$ and the RSD value was 14.27% . The value of the standard error of data measurement was determined with the flexible tool Error bar on the graph.

The LOD defined as $3 \times$ standard deviation of the blank, and at the LOQ defined as $10 \times$ standard deviation of the blank, divided to the slope (analytical sensitivity) of the calibration plot.

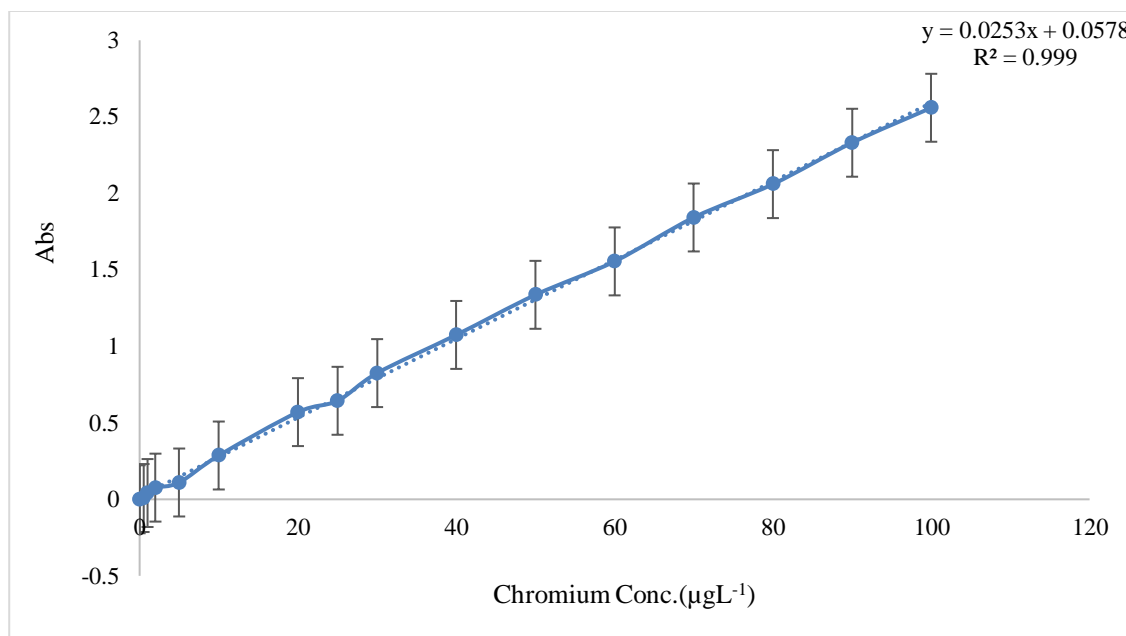


Fig. 10. Calibration Curve for Hexavalent Chromium (VI) in optimization Conditions by ETAAS method

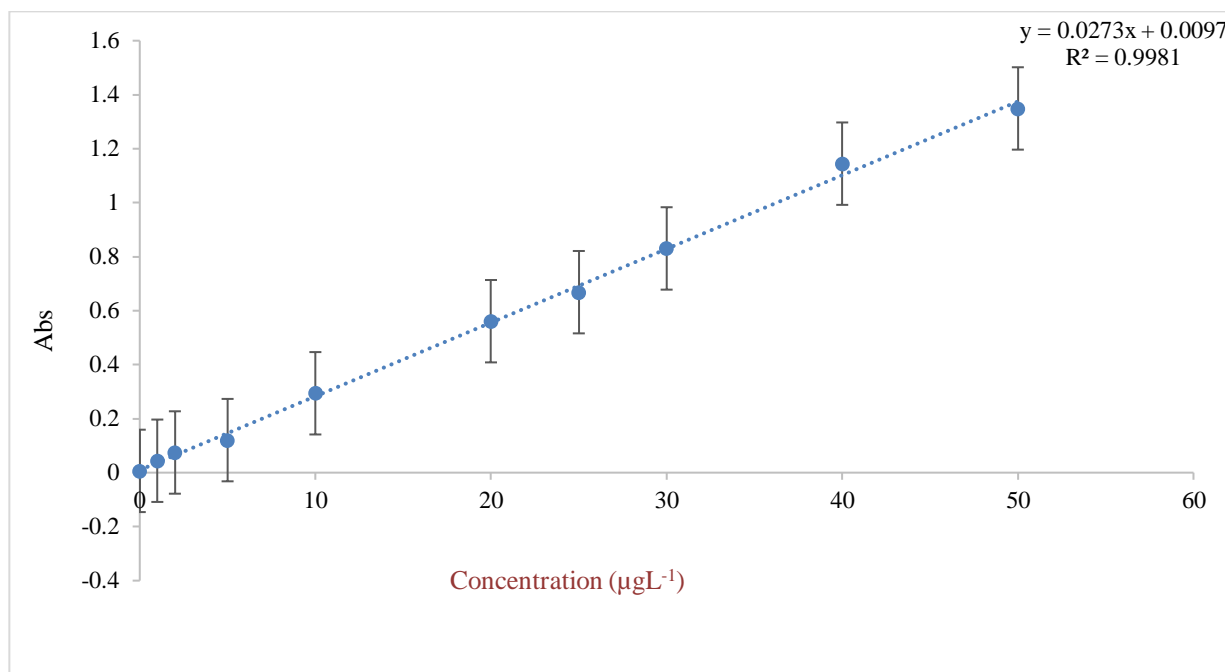


Fig. 11. Calibration Curve for Hexavalent Chromium (VI) in optimization Conditions by UV-Vis method

Table 7. Summary output and ANOVA by ETAAS method

Regression Statistics	
Multiple R	0.9996244
R Square	0.9992488
Adjusted R Square	0.9991952
Standard Error	0.025193
Observations	16

ANOVA						
	df	SS	MS	F	Significance F	Significance F < F
Regression	1	11.820462	11.82046	18624.03154	2.82726E-23	TRUE
Residual	14	0.0088856	0.000635			
Total	15	11.829347				

	Coefficients	Standard Error	t Stat	P-value	Lower 95%	Upper 95%	Lower 95.0%	Upper 95.0%		
Intercept	0.0196713	0.0093214	2.110327	0.053304236	-	0.039664	-0.0003212	0.0396638	TRUE	P-value >0/05
con.	0.0257149	0.0001884	136.4699	2.82726E-23	0.025311	0.026119	0.0253108	0.0261191	TRUE	P-value <0/05

Table 8. LINEST function by ETAAS method

b	0.0257149	0.019671303	a	ta	2.11032675	ta<t critical	TRUE
Sb	0.0001884	0.009321449	Sa	tb	136.4698924	tb>t critical	TRUE
R^2	0.9992488	0.025193028	Sr			t critical 14	2.16
F	18624.032	14	df				
SS	11.820462	0.008885641	residuals				

Table 9. The Real samples analysis

Sample	Spiked solution of Cr(μgL^{-1})	ETAAS			UV-Vis		
		Average absorbance	%Relative Recovery	STDEV A	Average absorbance	%Relative Recovery	STDEV A
Cr($30\mu\text{gL}^{-1}$)	-	0.821	-		0.829	-	
Water 1	-	0	-	0	0	-	0
	10	0.819	99.756	0.001	0.815	99.269	0.007
	100	0.826	100.609	0.003	0.836	101.827	0.0035
	500	0.804	97.929	0.008	0.798	97.199	0.0155
Water 2	-	0	-	0.4105	0	-	0.4145
	10	0.823	100.244	0.001	0.829	100.974	0
	100	0.826	100.609	0.003	0.833	101.462	0.002
	500	0.829	100.974	0.004	0.837	101.949	0.004
Water3	-	0.108	-	0.357	0.1	-	0.3605
	10	0.929	100.000	0.000	0.911	98.914	0.009
	100	0.932	100.323	0.002	0.940	102.063	0.0055
	500	0.961	103.445	0.016	0.955	103.692	0.013
Wastewater 1	-	1.1924	-	0.186	1.211	-	0.191
	10	1.986	98.639	0.014	1.991	97.982	0.0245
	100	1.999	99.285	0.007	1.988	97.835	0.026
	500	1.971	97.894	0.021	1.974	97.146	0.033
Wastewater 2	-	2.135	-	0.657	2.131	-	0.651
	10	2.947	99.696	0.004	2.920	98.916	0.02
	100	2.929	99.087	0.014	2.865	97.053	0.0475
	500	2.859	96.719	0.048	2.836	96.070	0.062
Wastewater 3	-	2.098	-	0.639	2.111	-	0.641
	10	2.918	99.966	0.000	2.915	99.420	0.0125
	100	2.916	99.897	0.001	2.882	98.295	0.029
	500	2.859	97.945	0.030	2.836	96.726	0.052
Treatment plant1	-	1.124	-	0.152	1.119	-	0.145
	10	1.922	98.817	0.012	1.914	98.660	0.017
	100	1.911	98.252	0.017	1.901	97.990	0.0235
	500	1.868	96.041	0.039	1.845	95.103	0.0515
Treatment plant2	-	1.124	-	0.152	1.117	-	0.144
	10	0.998	99.846	0.002	1.921	99.123	0.0125
	100	0.981	98.100	0.414	1.939	98.100	0.411
	500	0.965	96.500	0.005	1.922	96.500	0.012
Dam number 1	-	2.109	-	0.644	2	-	0.5855
	10	2.925	99.829	0.003	2.912	103.226	0.0415
	100	2.851	97.304	0.040	2.812	99.681	0.0085
	500	2.849	97.235	0.040	2.741	97.164	0.044
Dam number 2	-	1.148	-	0.164	1.125	-	0.148
	10	1.968	99.949	0.000	1.953	100.360	0.0005
	100	1.964	99.746	0.002	1.922	98.767	0.016
	500	1.907	96.851	0.031	1.872	96.197	0.041

Table 10. Effect of interfering Ions

Interference Ion	Interference to metal ion ratio(μgL^{-1})	ETAAS		UV-Vis	
		Abs	Recovery %	Abs	Recovery %
-	Just chromium ^a	0.824	-	0.83	-
pb	10.0	0.822	99.76	0.819	98.67
pb	100.0	0.849	103.03	0.851	103.28
pb	300.0	0.801	97.21	0.795	96.48
Zn	10.0	0.825	100.12	0.818	99.27
Zn	100.0	0.821	99.64	0.811	98.42
Zn	300.0	0.826	100.24	0.807	97.94
As	10.0	0.824	100.00	0.815	98.91
As	100.0	0.819	99.39	0.81	98.30
As	300.0	0.803	97.45	0.792	96.12
Ni	10.0	0.823	99.88	0.82	99.51
Ni	100.0	0.82	99.51	0.815	98.91
Ni	300.0	0.818	99.27	0.809	98.18
Co	10.0	0.827	100.36	0.822	99.76
Co	100.0	0.833	101.09	0.813	98.67
Co	300.0	0.835	101.33	0.801	97.21
Cd	10.0	0.832	100.97	0.827	100.36
Cd	100.0	0.821	99.64	0.808	98.06
Cd	300.0	0.817	99.15	0.802	97.33
Fe	10.0	0.826	100.24	0.819	99.39
Fe	100.0	0.835	101.33	0.841	102.06
Fe	300.0	0.814	98.79	0.804	97.57

^a Initial chromium standard solution concentration $30.0 \mu\text{gL}^{-1}$

In order to confirm the state of the calibration chart, the regression output was calculated using ANOVA (Table 7) and the LINEST function (Table 8) in the Excel environment. In these tables, df is the degree of freedom, SS is the fluctuation between the Y values calculated from the calibration line, MS is the mean square, and SS is the residual fluctuation between the observed Y values and the Y values obtained from the calibration line. The significance test F was used to evaluate the appropriate linear relationship between X and Y.

The standard deviation of the slope and width from the origin, the value of the slope and y - intercept, the regression standard deviation and the regression coefficient, F dispersion, degree of freedom, and the sum of squares based on the regression and the residual were calculated and confirmed in the LINEST function.

5. ANALYSIS OF REAL SAMPLES

Drinking water, wastewater, water sample behind the dam and water treatment plant samples were collected from different regions of the Khorasan-e-Razavi province and their analysis was performed according to the mentioned methodology by ETAAS. The standard solution $30 \mu\text{gL}^{-1}$ of chromium was considered. Then the standard concentrations of 10, 100 and 500 times

were added to the real samples. The recovery interval was calculated in the acceptable range of 96.041% to 103.445% and relative recovery values were attained in the range (95.103-103.692%) of UV-Vis method (Table 9).

6. INFLUENCE OF INTERFERING IONS

A solution of $30 \mu\text{gL}^{-1}$ standard chromium and interfering ions with different concentrations were used to investigate the effect of the interfering ions. Samples were analyzed using graphite furnace atomic absorption spectrometry. The maximum recovery range of chromium and its tolerable concentrations ($10, 100, 300 \mu\text{gL}^{-1}$ of interfering ions) are shown in Table 10. The recovery range was found in the acceptable range of 97.21% to 103.03% by ETAAS Method and the recovery range was found in the acceptable range of 96.48 to 103.25% by UV-Vis Method.

7. CONCLUSION

In this research project, commercial and inexpensive sodium bentonite, and nano bentonite prepared from two commercial types of bentonites are used as the adsorbents to remove chromium ions from real samples such as drinking water, wastewater, water sample behind the dam and treatment plant samples, along with the ETAAS and UV-VIS method. The advantages of this method include the good removal effectiveness of

this mineral pollutant, repeatability, sensitivity, compatibility with the environment, and its economic efficiency. Using the Mini tab 20 software, all optimization steps were performed using the Plackett-Burman (PBD) design and the central compound design (CCD) method. Chromium calibration curve was drawn in optimal conditions by plotting the absorbance against the standard concentrations. Detection limit and quantification limit, linear dynamic range and correlation coefficient were obtained for chromium by two mentioned methods.

REFERENCES

- [1] M. Zessner, Monitoring, Modeling and Management of Water Quality. *Water* 13 (2021)1523.
- [2] R.J. Vitale CPC, G.R. Mussoline, K.A. Rinehimer, Environmental Monitoring of Chromium in Air, Soil, and Water, *R. T. P.* 26 (1997) S80-S85.
- [3] M. B. Rajkovic, C. M. Lacnjevac, N.R. Ralevic, M.D. Stojanović, D.V. Tosković, G.K. Pantelic, N. M. Ristic, S. Jovanic, Identification of metals (heavy and radioactive) in drinking water by an indirect analysis method based on scale tests, *Sensors (Basel)*8 (2008) 2188-2207.
- [4] M. Qasim, Biodegradation of hexavalent chromium (Cr^{+6}) in wastewater using *Pseudomonas* sp. and *Bacillus* sp. bacterial strains, *I.J.E.E.* 4 (2013) 653-662.
- [5] G. Qin, M. J. McGuire, N. K. Blute, C. Seidel and L. Fong, Hexavalent chromium removal by reduction with ferrous sulfate, coagulation, and filtration, *Environ. Sci. Technol* 39 (2005) 6321-6327.
- [6] B. Pakzadeh and J. R. Batista, Chromium removal from ion-exchange waste brines with calcium polysulfide, *Water research* 45(2011) 3055-3064.
- [7] A. A. Atia, Synthesis of a quaternary amine anion exchange resin and study its adsorption behaviour for chromate oxyanions, *J. Hazard. Mater*137 (2006) 1049-1055.
- [8] X. -q. Li, D. W. Elliott and W. -x. Zhang, Zero-valent iron nanoparticles for abatement of environmental pollutants: materials and engineering aspects, *J. Hazard. Mater*31 (2006) 111-122.
- [9] Y. Liu, T. Phenrat and G. V. Lowry, Effect of TCE concentration and dissolved groundwater solutes on NZVI-promoted TCE dechlorination and H_2 evolution, *Environ. Sci. Technol.* 41(22) (2007) 7881-7887,
- [10] Ç. Üzümlü, T. Shahwan, A. E. Eroğlu, K. R. Hallam, T. B. Scott and I. Lieberwirth, Synthesis and characterization of kaolinite-supported zero-valent iron nanoparticles and their application for the removal of aqueous Cu^{2+} and Co^{2+} ions, *Appl. Clay Sci.* 43 (2009) 172-181,
- [11] K. G. Bhattacharyya and S. S. Gupta, Adsorption of a few heavy metals on natural and modified kaolinite and montmorillonite: a review, *Adv. Colloid Interface Sci.* 140 (2008)114-131.
- [12] A. Daley, H. Stokes-Lampard and C. MacArthur, Exercise to reduce vasomotor and other menopausal symptoms: a review, *Maturitas* 63(3) (2009)176-180,
- [13] M. Alzamel, M.Fall, S. Haruna, Swelling ability and behaviour of bentonite-based materials for deep repository engineered barrier systems: Influence of physical, chemical and thermal factors, *J. R. M. G. E.* 14 (2022) 689-702,
- [14] A. Rawat, W. Baille, S. Tripathy, Swelling behavior of compacted bentonite-sand mixture during water infiltration, *Eng. Geol.* 257 (2019) 105141
- [15] A.H. Elgarhy, B.N. A. Mahran, G. Liu, T. A. Salem, E.S. ElBastamy ElSayed, L. A. Ibrahim, Comparative study for removal of phosphorus from aqueous solution by natural and activated bentonite, *Sci. Rep.* 12 (2022) 19433
- [16] B. Butcher, The advantages of a salt/bentonite backfill for Waste Isolation Pilot Plant disposal rooms, MRS Online Proceedings Library (OPL), MRS Online Proceedings Library (OPL) , MRS Online Proceedings Library (OPL) Symposium V, *S. B. N. W. M XVII.* 333 (1993) 911.
- [17] C. Boswell, B. Swanney and W. Owers, Sulfur/sodium bentonite prills as sulfur fertilizers. 2. Effect of sulfur-sodium bentonite ratios on the availability of sulfur to pasture plants in the field, *J. fertil. pestic.* 15 (1988) 33-45.
- [18] A. Muscolo, T. Papalia, G. Settineri, C. Mallamaci and M. R. Panuccio, Sulfur bentonite organic based fertilizers as tool for improving bio compounds with antioxidant activities in red onion, *J. Sci. Food Agric. J SCI FOOD AGR.* 100 (2020) 785-793.
- [19] M. Önal, Y. Sarıkaya, Preparation and characterization of acid-activated bentonite powders, *Powder Technol.*172 (2007) 14-18.
- [20] Z. Darvishi and A. Morsali, Synthesis and characterization of Nano-bentonite by sonochemical method, *Ultrason. Sonochem.*18 (2011)238-242,
- [21] R. Naseem and S. Tahir, Removal of Pb (II) from aqueous/acidic solutions by using bentonite as an adsorbent, *Water research.*35 (2001) 3982-3986.
- [22] A. Salihu, M. Z. Alam, M. I. AbdulKarim and H. M. Salleh, Optimization of lipase production by *Candida cylindracea* in palm oil mill effluent based medium using statistical experimental design, *J. Mol. Catal. B Enzym.* 69 (2011) 66-73,
- [23] G. Ruchi, G. Anshu and S. Khare, Lipase from solvent tolerant *Pseudomonas aeruginosa* strain: production optimization by response surface methodology and application, *Bioresour. Technol.* 99 (2008) 4796-4802,

- [24]A. Nezhadali, M. O. Motlagh and S. Sadeghzadeh, Spectrophotometric determination of fluoxetine by molecularly imprinted polypyrrole and optimization by experimental design, artificial neural network and genetic algorithm, *S. A. A.* 190 (2018) 181-187,
- [25]C. Hall, J. Kelly, H. Whitlock and L. Ritchie, Prolonged anthelmintic effect of closantel and disophenol against a thiabendazole selected resistant strain of *Haemonchus contortus* in sheep, *Res. Vet. Sci.*31 (1981) 104-106.
- [26]R. Woestenborghs, J. Hendrickx, L. Michielsen and J. Heykants, Quality assurance in the food control microbiological laboratory, *FAO Food and Nutrition.* 41 (1992) 15, 103053-7.
- [27]C. Fernandes, C. Catrinescu, P. Castilho, P. Russo, M. Carrott and C. Breen, Catalytic conversion of limonene over acid activated Serra de Dentro (SD) bentonite, *APPL CATAL A-GEN* .318 (2007) 108-120.
- [28]R. S. Hebbar, A. M. Isloor, B. Prabhu, A. M. Asiri and A. Ismail, Removal of metal ions and humic acids through polyetherimide membrane with grafted bentonite clay, *Sci. Rep.* 8 (2018) 4665.
- [29]D. Chattopadhyay, A. K. Mishra, B. Sreedhar and K. Raju, Thermal and viscoelastic properties of polyurethane-imide/clay hybrid coatings, *Polym. Degrad. Stab.*91 (2006) 1837-1849,
- [30]N. Banik, S. Jahan, S. Mostofa, H. Kabir, N. Sharmin, and M. Rahman, Synthesis and characterization of organoclay modified with cetylpyridinium chloride, *Bangladesh Journal of J. Sci. Ind. Res.*50 (2015) 65-70.
- [31]J. T. Klopogge, Spectroscopic studies of synthetic and natural beidellites: A review, *Appl. Clay Sci.* 31 (2006) 165–179.
- [32]M. Hayati Ashtiani, Characterization of nano porous bentonite (montmorillonite) particles using FTIR and BET BJH analyses, *Part Part Syst Charact.* 28 (2011) 71-76,



COPYRIGHTS

© 2022 by the authors. Licensee PNU, Tehran, Iran. This article is an open access article distributed under the terms and conditions of the Creative Commons Attribution 4.0 International (CC BY4.0) (<http://creativecommons.org/licenses/by/4.0>)

حذف جذبی سازگار با محیط زیست کروم از آب و فاضلاب توسط نانو بنتونیت سدیم

مریم امیدوار مطلق، زرین اسحاقی، حسن علی حسینی*

بخش شیمی، دانشگاه پیام نور، تهران، ایران

* E-mail: shahosseini57@pnu.ac.ir

تاریخ پذیرش: ۱۶ مهر ۱۴۰۲

تاریخ دریافت: ۱۲ شهریور ۱۴۰۲

چکیده

آلودگی منابع آب به کروم به دلیل استفاده گسترده از آن در صنعت به یک مشکل فراگیر جهانی تبدیل شده است. در این تحقیق از بنتونیت سدیم تجاری ارزان قیمت و نانو بنتونیت سنتز شده برای حذف یون های کروم از محلول های آبی به همراه طیف سنجی جذب اتمی الکترو حرارتی (ETAAS) و طیف سنجی فرا بنفش - مرئی (UV-Vis) استفاده شد. مورفولوژی نمونه های بنتونیت با استفاده از آنالیزهای XRD، FTIR و میکروسکوپ الکترونی روبشی (SEM) مورد بررسی قرار گرفت. برای غربالگری اهمیت نسبی متغیرها، پارامترهایی از جمله pH، زمان جذب، مقدار جاذب، حجم حلال و اجذب و سرعت همزدن با استفاده از طراحی پلاکت -یورمن با استفاده از نرم افزار مینی تب ۲۰ مورد بررسی قرار گرفت. در ادامه، بهینه سازی با استفاده از طرح مرکب مرکزی (CCD) انجام شد و پاسخ ها مورد ارزیابی قرار گرفتند. منحنی کالیبراسیون با رسم ابزوریانس در برابر غلظت استاندارد رسم شد. محدوده دینامیکی خطی ۰.۰۰۳ تا ۱۰۵ میکروگرم بر لیتر (DLR) و ضریب همبستگی 0.999 (R2) برای کروم به دست آمد. حد تشخیص (LOD) و حد کمی (LOQ) برای کروم به ترتیب برابر با ۰.۰۰۲ و ۰.۰۰۳۹ میکروگرم بر لیتر به دست آمد. انحراف استاندارد نسبی (RSD) ۶.۹۳ درصد و بازیابی نسبی برای کروم در نمونه های واقعی در محدوده ۹۶.۰۴۱ تا ۱۰۳.۴۴۵ درصد برای روش ETAAS به دست آمد. مقادیر حد تشخیص (LOD) و حد کمی (LOQ) به روش UV-Vis به ترتیب ۰.۰۰۷ و ۰.۰۲۱ میکروگرم در لیتر و محدوده خطی دینامیکی (DLR) ۰.۰۰۵ تا ۵۰ میکروگرم در لیتر با ضریب همبستگی (R2) ۰.۹۹۸ بود. انحراف استاندارد نسبی (RSD) ۲۷.۱۴ درصد و بازیابی نسبی این روش در نمونه های واقعی از ۹۵/۱۰۳ درصد تا ۱۰۳/۶۹۲ درصد رسیده است.

کلید واژه ها

طیف سنجی جذب اتمی الکتروحرارتی؛ طیف سنجی فرابنفش مرئی؛ نانو بنتونیت سدیمی؛ کروم.